buildings

MDPI

Article

Utilizing Low Yield Point Steel to Improve the Behavior of the I-Shaped Shear Links as Dampers

Ali Ghamari [1], Chanachai Thongchom [2,*], Ramadhansyah Putra Jaya [3,*] and Thandiwe Sithole [4]

[1] Department of Civil Engineering, Ilam Branch, Islamic Azad University, Ilam 1477893855, Iran
[2] Department of Civil Engineering, Faculty of Engineering, Thammasat School of Engineering, Thammasat University, Pathumthani 12120, Thailand
[3] Faculty of Civil Engineering Technology, Universiti Malaysia Pahang, Kuantan 26300, Malaysia
[4] Department of Chemical Engineering, The University of Johannesburg, P.O. Box 17011, Doornfontein 2088, South Africa
* Correspondence: tchanach@engr.tu.ac.th (C.T.); ramadhansyah@ump.edu.my (R.P.J.)

Abstract: Concentrically braced frame (CBF) systems are susceptible to buckling (which causes a decrease in energy absorption), although this system has considerable lateral stiffness and strength. To over this shortcoming, researchers have suggested the use of I-shaped steel dampers as a practical idea that prevents buckling and increases the energy absorption but reduces the stiffness of the system. To increase the stiffness of the damper, the thickness of the web or the thickness of the flange can be increased, but by increasing their thickness the shear capacity of the damper also increases. Nevertheless, with the increase in the capacity of the damper, the forces created in the elements outside the damper will also increase, which is usually not a suitable solution. Therefore, in this paper, the use of the low yield point for the web plate of an I-shaped damper is proposed to compensate for it. Accordingly, its behavior is investigated parametrically and numerically and also requires equations to design the system proposed. Results indicated that utilizing an LYP damper improves the behavior of the system in the case of energy absorption, stiffness, and strength. Comparing the LYP damper and the conventional I-shaped damper (made of A36 steel) reveals that both dampers pertain to stable hysteresis loops without any degradation, which confirms the capability of the I-shaped damper to dissipate seismic energy. Although the flange plate properties contribute to the load-bearing of the damper, the A36 damper is more affected by the flange plate than the LYP damper that is concluded for LYP dampers the flange plate contribution in the shear strength of the damper is ignorable at the beginning of imposed loading.

Keywords: shear damper; LYP steel; CBF braces; stiffness; energy absorption

Citation: Ghamari, A.; Thongchom, C.; Putra Jaya, R.; Sithole, T. Utilizing Low Yield Point Steel to Improve the Behavior of the I-Shaped Shear Links as Dampers. *Buildings* **2023**, *13*, 554. https://doi.org/10.3390/buildings13020554

Academic Editor: Harry Far

Received: 16 January 2023
Revised: 10 February 2023
Accepted: 15 February 2023
Published: 17 February 2023

1. Introduction

Although concentrically braced frames (CBFs) have been introduced as a system with the highest stiffness and strength in comparison with other conventional systems, they have suffered from low dissipating energy capability. This shortcoming is due to the susceptibility of the diagonal member element of CBF to buckling under cyclic loading. This phenomenon leads the hysteresis curve of the CBF system to degradation. Therefore, the system does not exhibit ductile behavior under seismic loading. In contrast, the eccentrically braced frames (EBFs) have shown a suitable performance under seismic loading in past earthquakes [1,2] as well as experimental [3,4] and numerical studies [5,6]. Since the horizontal link is a part of the floor beam, repairing the EBF after a severe earthquake is complicated. Moreover, in this system, the shear capacity of the link beam creates substantial axial forces to the columns surrounding the brace, which should be included in the seismic design and analysis process [7,8]. Moreover, when a horizontal link is attached to a column, in addition to the axial force, a large shear force is imposed on the column, which has been studied to overcome the problem [9]. Utilizing a vertical shear link in an

EBF system (V-EBF) attached under the floor beam (between the floor beam and the brace elements), the problem is solved. The link in this system does not subject to axial loading. In other words, the influence of axial forces on the vertical links is negligible [10]. Also, the V-EBF system is used as an alternative strategy for seismic improvement and retrofitting of reinforced concrete buildings [11]. In line with utilizing the V-EBF, some researchers have proposed the use of metallic dampers to improve the behavior of CBF braces such as added damping and stiffness (ADAS) dampers [12], ellipse added damping and stiffness (EDAS) dampers [13], triangular added damping and stiffness (TADAS) [14], curved-TADAS [15], U-shaped dampers [16], box-shaped dampers [17], ring damper [18], flexural dampers [19], shear dampers [20,21], shear dampers strengthened with X-stiffeners [22,23], and braced ductile shear panels [24]. Among existing steel dampers, shear dampers are more popular than other dampers due to their simplicity in construction, ease of installation, ease of replacement after an earthquake, and also favorable performance confirmed by numerical and laboratory studies. By adding the damper to the element brace directly, stiffness is obtained from the sum of the stiffness series of equivalent springs. Accordingly, although the shear dampers directly connected to the braces prevent the buckling of the diagonal member of the CBF and increase its energy absorption capability, they also reduce the elastic stiffness of the system.

Some researchers investigated the low yield point (LYP) shear panels [25,26]. Okazaki and Engelhardt [27] conducted various experiments on the cyclic loading behavior of LYP-EBF links made of rolled W-shaped samples with ASTM A992 steel. They proposed to use Ω = 1.35 to 1.41, which was lower than AISC 341-16 [28] and ANSI/AISC 360-16 [29]. However, a greater overstrength factor is possibly required for very short links with heavy flanges [30]. Sabouri-Ghomi [31], confirmed the omittance of local bucking in the shear links using easy-going steel (EGS) has better performance in cyclic behavior than a link constructed from ST37 steel. An interesting finding revealed by Dusicka et al. [32] was that the cyclic behavior and shear deformation of links made from LYP steel showed noticeable superiority over common structural designs. This was accomplished through the alternation of failure mode realized by a small value of web compactness.

As mentioned before, adding a damper to the CBF braces reduces the stiffness of the system, although it improves the behavior of the system in terms of energy absorption and ductility. To overcome this shortcoming, the thickness of the damper can be increased, but its capacity will also increase. Accordingly, the force created in the elements outside the damper is also increased. Therefore, in this paper, an I-shaped shear damper is proposed, which pertains to ease of construction and ease of replacement after a severe earthquake. The proposed damper is a compound of LYP steel for the web plates and A-36 steel for the flange plates. By keeping the shear strength of the I-shaped damper constant, its thickness can be increased to compensate for the stiffness (caused by adding the damper to the brace).

2. The Proposed Shear Link

Although the suitable performance of the damper under seismic loading accounted as the important role of the damper, easy fabrication, easy installation, and easy replacement after an earthquake are the other important roles regarding dampers. The presented damper in this paper pertains to these advantages. As illustrated in Figure 1, the shear damper made of a main web plate with LYP steel surrounded by two end flange plates formed an I-shaped damper. It is attached at the end of a diagonal CBF brace element. It is expected that the damper will yield before the buckling of the diagonal brace element. Therefore, it acts as a ductile fuse and pertains easy replacement after a severe earthquake due to its easy fabrication.

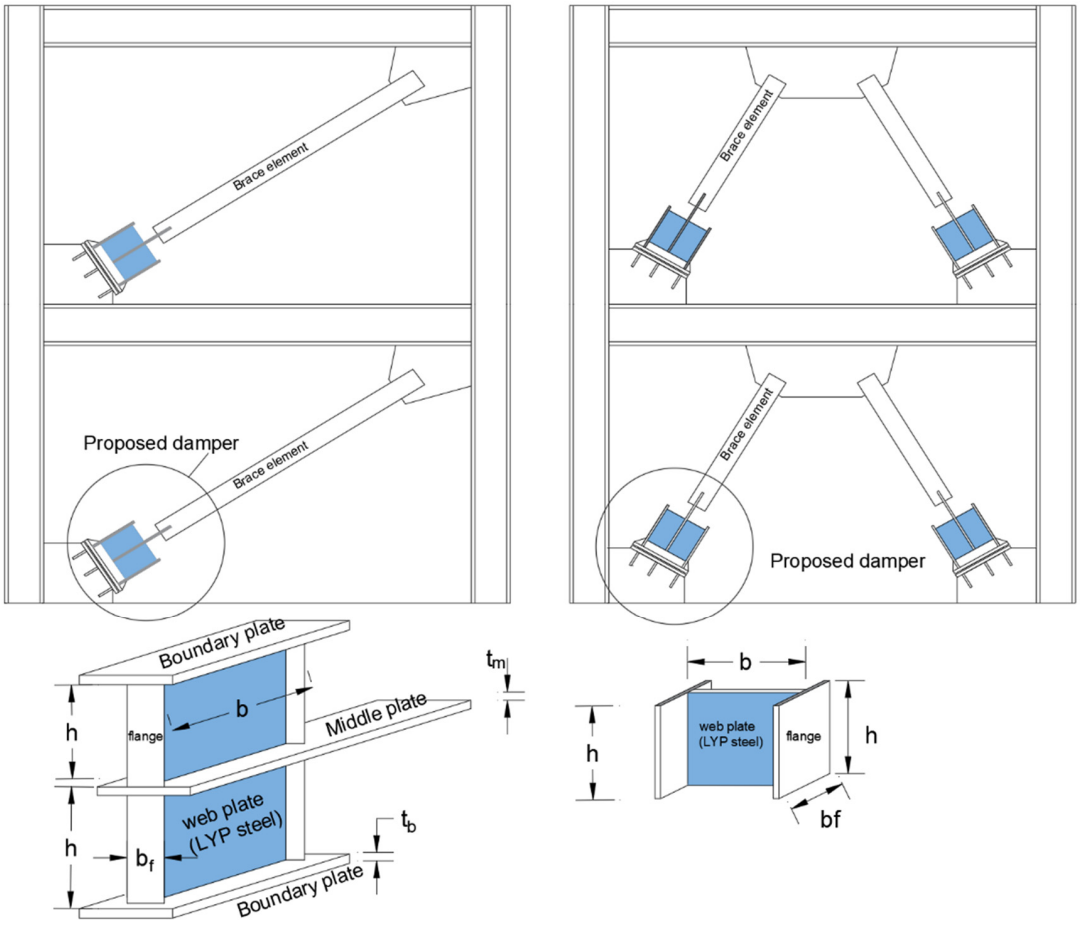

Figure 1. Proposed damper.

The LYP steel, which has a lower yield strength than A36 steel and a great elongation property, is preferred to offset the increase in web area to achieve the desired yield strength and high stiffness for the damper. Subsequently, the advantages of utilizing LYP steel in comparison with carbon steel are summarized in two points: (1) the shear displacement of the system with LYP steel is lower than conventional steel whereas both systems have equal strength and (2) the ductility and capability of energy dissipating the LYP steel are much greater than conventional steel. Recently, LYP steel shear links with/without web stiffeners have introduced a series of problems [30]. In addition, some large overstrength factors are observed in certain studies, as in the work by Dusicka et al. [32].

According to the AISC AISC 341-16 [28], the performance of the shear I-shaped links is categorized into three types: the shear mechanism by $\rho < 1.6$, the shear–flexural mechanism by $1.6 < \rho < 2.6$, and the flexural mechanism by $\rho > 2.6$, where $\rho = \frac{e}{M_p/V_p}$. Comprehensive outcomes were reported by Kasai and Popov [33], Hjelmstad and Popov [34], Engelhardt and Popov [35], and Okazaki. Refs. [7,27,36] have confirmed that an appropriately designed shear link can provide stable predictable ductile behavior under cyclic loading.

Regarding I-shaped links, AISC 341-16 [28] presented Equation (1) to calculate the shear strength for shear links ($\rho < 1.6$). Article F3.5b.2 of AISC 341-16 is used to determine the design shear strength, $\phi_v V_n$. For an I-shaped shear link ($\rho < 1.6$), $V_n = V_P$, where V_P is calculated as indicated in Equation (1):

$$V_p = 0.6 F_{yw} A_w \tag{1}$$

where the net area section of the web, A_w, equals $t_p\left(d - t_f\right)$. It should also be noted that certain AISC 360-16 [29] specifications define V_P, where h is replaced by d.

This paper assumes that the shear capacity of I-shaped shear links is provided by web and flange plates. Since two I-shaped shaped links are used for constructing the damper, a coefficient of 2 is applied:

$$V_u = 2(V_p + V_f) \tag{2}$$

Although AISC specifications recommend calculating the nominal shear capacity of short links based on the web area, without including the contribution of the flanges, according to findings by McDaniel et al. [37], in short links, the flanges are also subject to significant shear loading. Manheim and Popov [38] and Richards [39] propose that the flange should be considered in determining the plastic shear capacity of the link. Since shear loading is also applied to the flanges, Equation (1) is revised to consider the shear strength of the flanges:

$$V_p = \eta 0.6 F_{yw}(b + 2t_f)t_p \tag{3}$$

In this equation, to consider the effect of strain hardening, it is proposed that η be equal to 1.1. The upper bound of the equation establishes when four flexural plastic hinges are formed in the flange plates. Hinges are formed when the moment reaches the plastic moment. To satisfy the equilibrium, Equation (4) should be established:

$$V_f = \frac{4M_{pf}}{h} \tag{4}$$

where $M_{pf} = \frac{b_f t_f^2}{4} F_{yf}$. Additionally, Equation (2) is simplified as $V_p = 2\left(\eta 0.6(b + 2t_f)t_p F_{yw} + \frac{b_f t_f^2}{4} F_{yf}\right)$, accordingly, it is rewritten as:

$$V_n = 1.2\eta(b + 2t_f)t_p F_{yw} + \frac{b_f t_f^2}{2} F_{yf} \tag{5}$$

Correspondingly, it is assumed that both web plate and flange plates contribute to the stiffness of the damper. In other words, the stiffness of the damper includes the stiffness of the web plate and the stiffness of the flange plates as $K = 2(K_p + K_f)$. Factor 2 is regarding the two I-shaped dampers used. Since web plates act as shear plates, and knowing the $E = 2G(1 + v)$ while Poisson ratio of steel equals 0.3, the web plate stiffness is given by:

$$K_p = \frac{GA_w}{h} = \frac{E}{2.6}\frac{t_p b}{h} \tag{6}$$

Moreover, the flange plate stiffness is obtained

$$K_f = \frac{24EI}{h^3} = 2Eb_f\left(\frac{t_f}{h}\right)^3 \tag{7}$$

Therefore, the stiffness of the proposed damper is suggested as:

$$K = 2E\left(\frac{t_p b}{2.6h} + 2b_f\left(\frac{t_f}{h}\right)^3\right) \tag{8}$$

3. Method of Study

The innovative idea in this article is to use the web made of LYP100 steel. In LYP100 steel, its yield strength and modulus of elasticity are, respectively, about 2.35 times and 30% lower than A36 steel. Therefore, by keeping constant the shear capacity of the damper, the thickness can be increased by 2.35 times without creating additional force in the external elements of the damper. Referring to Equations (5) and (8), both the shear strength and the stiffness of the damper are related to the thickness of I-shaped plates and their mechanical properties. Accordingly, considering that the thickness can be increased by 2.35 times, the stiffness of the damper is expected to increase and, due to its lower yield stress, its energy

absorption is expected to improve. Subsequently, in the present paper, the behavior of bare dampers is investigated.

4. Numerical Study

4.1. Modeling

To simulate the FE models, ANSYS software using SHELL 181 was used. The element has the capability of accounting for the large displacement, buckling, and material nonlinearity. Although solid (brick) elements can be used to simulate the damper, it increases the time of analysis. Additionally, the same results are obtained and the capability of the element is verified in the next section, thus the SHELL 181 was used. Figure 2 shows a schematic view of an FE model. For each damper, a mesh that includes 1724 elements was used. To do so, each web was divided by $20 \times 20 = 400$ elements (400 elements for two webs) and each flange was created as $4 \times 20 = 80$ (320 elements for four flanges). The nonlinearity (material, and geometric) was considered in this paper. Material nonlinearity was measured by defining the stress–strain of the material and geometric nonlinearity was considered by applying imperfection. To determine the imperfection, first, a buckling analysis was performed, then the FE model was updated based on the buckled model. As a result, the first positive eigenmode of each link was amplified by a very small magnitude of h/10,000 and was then used as the initial shape for nonlinear analysis. A convergence study was performed on a sample incorporating the smallest values for the thickness and the web panel.

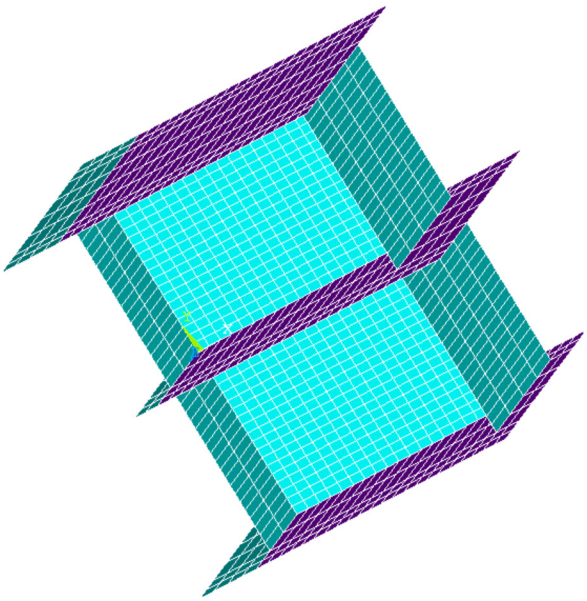

Figure 2. A schematic view of FE models.

4.2. Verification of the FE results

An experimental test specimen performed by Engelhardt and Popov [35] was selected to verify the FE results. This specimen was made of A36 material, with dimensions of W18 × 40 and a length of 711 mm. The links used for this experimental test have the same boundary condition as the dampers proposed in this paper. Consequently, the boundary conditions and mechanisms employed in the experimental test were the same as those for the proposed damper. A comparison of the deformation and hysteresis curve results of the FE modeling with the results obtained in the experimental test reveals good agreement and accuracy of the FE modeling, Figure 3. According to the figure, the slope of the curves (stiffness) obtained from the FE analysis is consistent (with a maximum error of 2%) with the experimental test results. Additionally, the shear capacity obtained from the FE results is associated with the experimental test results with a maximum error of 5%, which indicates a good agreement between the numerical results and the finite element results. Additionally,

the yielding status of the test and the FE results is the same. The good agreement between the FE and experimental results confirms that the FE results are accurate enough to proceed with the other FE modeling in this paper.

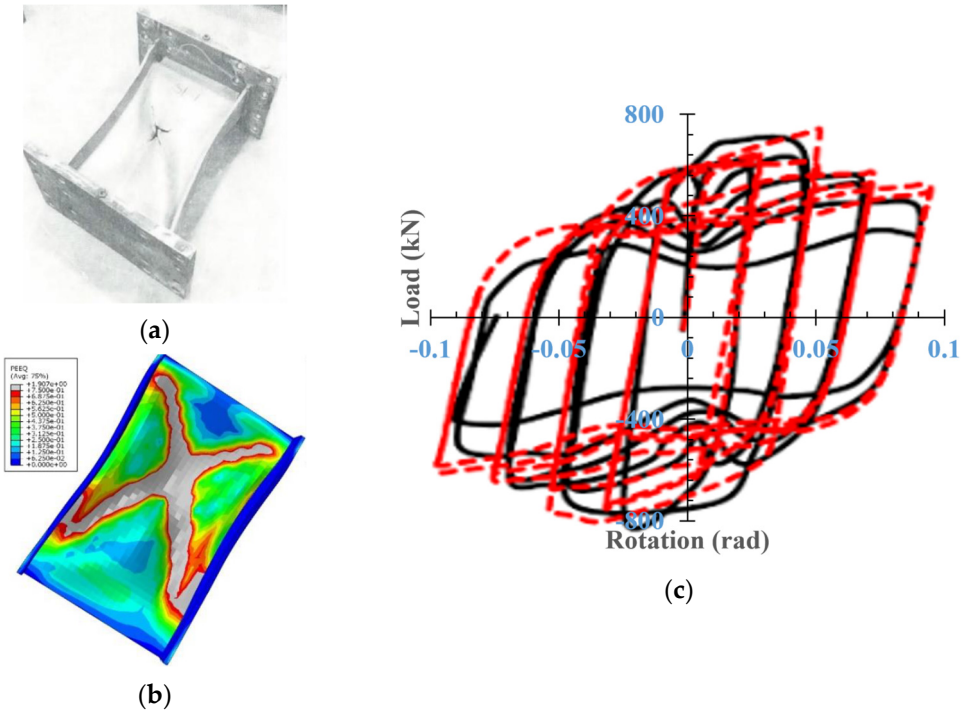

Figure 3. Comparison of results of the FE modeling and the experimental test. (**a**) The shear link at the end of testing [35]; (**b**) FE simulation; (**c**) comparing the hysteresis curves.

4.3. Boundary Conditions and Material Properties

The boundary condition was imposed to create the same condition when the damper is located in the frame. To do so, the end of the boundary plates of the damper, where they attached to the guest plate, was restricted against rotation and displacement. Additionally, the other end of the damper was not restricted. Additionally, loading was applied to the middle plate at the other end damper. The dampers were applied load up to reach a rotation of 8% (0.08 radians), as specified in article F3.4a of AISC 341-16 [28], and short shear links attain a maximum rotation of 0.08 rad under design seismic loading. In the cyclic analysis, the cyclic loading by ATC 24 [40] protocol loading guidelines was applied to the dampers. Accordingly, to achieve the 0.08 radian, the displacement equal to 11.2, 16.8, 22.4, and 28 mm, respectively, was applied to the models with h = 140, 210, 280, and 350 mm. The material properties used in this paper are listed in Table 1. The properties were chosen as reported in Ref. [30].

Table 1. Material properties [30].

Materials	Fy (MPa)	Fu (MPa)	Modulus of Elasticity (GPa)
LYP100	100	257	153
A36	235	360	200

5. Parametric Study

As explained in the method of the study section, two types of dampers—LYP dampers (I-shaped damper made of LYP steel for web plat) and A-36 dampers (I-shaped damper made of A36 steel)—are investigated. For the parametric study, the FE models were designed as shown in Table 2. Since the shear capacity tends to be kept constant, the same Fwyb.tw is used for both dampers. To do so, for all models b = 200 mm was selected. For

all A36 dampers, the tp equals 6 mm was designed and increased to 14 mm (as the ratio of $\frac{F_{yw(A36)}}{F_{yw(LYP)}} = \frac{235}{100} = 2.35$ where $2.35 \times 6 = 14$) for LYP steel.

Table 2. Properties of the models for the parametric study.

FE Model (ρ-ψ-t_f-h)	h (mm)	t_p (mm)	t_f (mm)	ρ	ψ	Web Plate Material
L-0.21-6.3-10-140	140	14	10	0.21	6.30	LYP
L-0.15-2.8-15-140	140	14	15	0.15	2.80	LYP
L-0.12-1.58-20-140	140	14	20	0.12	1.58	LYP
L-0.10-1.00-25-140	140	14	25	0.10	1.01	LYP
L-0.08-0.7-30-140	140	14	30	0.08	0.70	LYP
L-0.32-9.45-10-210	210	14	10	0.32	9.45	LYP
L-0.23-4.2-15-210	210	14	15	0.23	4.20	LYP
L-0.18-2.36-20-210	210	14	20	0.18	2.36	LYP
L-0.15-1.51-25-210	210	14	25	0.15	1.51	LYP
L-0.12-1.05-30-210	210	14	30	0.12	1.05	LYP
L-0.42-12.6-10-280	280	14	10	0.42	12.60	LYP
L-0.31-5.6-15-280	280	14	15	0.31	5.60	LYP
L-0.24-3.15-20-280	280	14	20	0.24	3.15	LYP
L-0.19-2.02-25-280	280	14	25	0.19	2.02	LYP
L-0.16-1.4-30-280	280	14	30	0.16	1.40	LYP
L-0.53-15.75-10-350	350	14	10	0.53	15.75	LYP
L-0.38-7.0-15-350	350	14	15	0.38	7.00	LYP
L-0.30-3.94-20-350	350	14	20	0.30	3.94	LYP
L-0.24-2.52-25-350	350	14	25	0.24	2.52	LYP
L-0.20-1.75-30-350	350	14	30	0.20	1.75	LYP
140-10-0.25-6.3	140	6	10	0.25	6.30	A36
140-15-0.18-2.8	140	6	15	0.18	2.80	A36
140-20-0.13-1.58	140	6	20	0.13	1.58	A36
140-25-0.11-1.00	140	6	25	0.11	1.01	A36
140-30-0.10-0.7	140	6	30	0.09	0.70	A36
210-10-0.38-9.45	210	6	10	0.38	9.45	A36
210-115-0.26-4.2	210	6	15	0.26	4.20	A36
210-20-0.2-2.36	210	6	20	0.20	2.36	A36
210-250-0.16-1.51	210	6	25	0.16	1.51	A36
210-30-0.13-1.05	210	6	30	0.13	1.05	A36
280-10-0.51-12.6	280	6	10	0.51	12.60	A36
280-15-0.35-5.6	280	6	15	0.35	5.60	A36
280-20-0.26-3.15	280	6	20	0.26	3.15	A36
280-25-0.21-2.02	280	6	25	0.21	2.02	A36
280-30-0.17-1.4	280	6	30	0.17	1.40	A36
350-10-0.64-15.75	350	6	10	0.64	15.75	A36
350-15-0.44-7.0	350	6	15	0.44	7.00	A36
350-20-0.33-3.94	350	6	20	0.33	3.94	A36
350-25-0.26-2.52	350	6	25	0.26	2.52	A36
350-30-0.22-1.75	350	6	30	0.22	1.75	A36

h—height of damper. t_f—the flange plate thickness. t_p—the web plate thickness. ψ—the ratio of the web plate capacity divided by the flange plate capacity.

A constant capacity of web plate strength (and constant Aw for A36 and LYP) was maintained to have a clear comparison between the designed models. Since other parameters such as flange plates properties are expected to affect the behavior of the dampers, different t_f was considered to evaluate the effect of the defined ψ parameter as $\psi = \frac{V_p}{V_f}$. where Vp is obtained from Equation (1) and Vf is the ultimate shear strength of the flange, given by Equation (4). Additionally, for all models, bf = 160 mm is used. Although AISC 341-16 [28] classifies links with $\rho < 1.6$ as shear links, the effect of ρ (even lower than 1) is

considered. For ρ = e/(MP/VP), the Vp is calculated by Equation (1) and e = b and M_p is determined as:

$$M_p = F_{yf} b_f t_f b + \frac{F_{yw} t_w h^2}{4} \quad (9)$$

Subsequently, the designed name of each model includes five parts as L or A-ρ-ψ-t_f-h. The first part indicates the L for LYP or A for A36 used for the web plate of the damper. The other parts' values used for the parameters are variables considered in the parametric study.

6. Results and Discussion

6.1. Hysteresis Curves

The hysteresis curves of the dampers with t_f = 10 mm and t_f = 30 mm as dampers with the thinnest and thickest flange plates are compared in Figure 4. In this figure, for summarizing the results, only dampers with h = 140 and 350 mm are shown. Results indicate that all dampers show stable hysteresis loops without any degradation. Correspondingly, the LYP dampers pertain better performance than A36 dampers in the case of energy absorption, ultimate strength, and stiffness. Furthermore, by increasing the t_f and reducing h, the energy absorption of the damper is improved for both LYP dampers and A36 dampers.

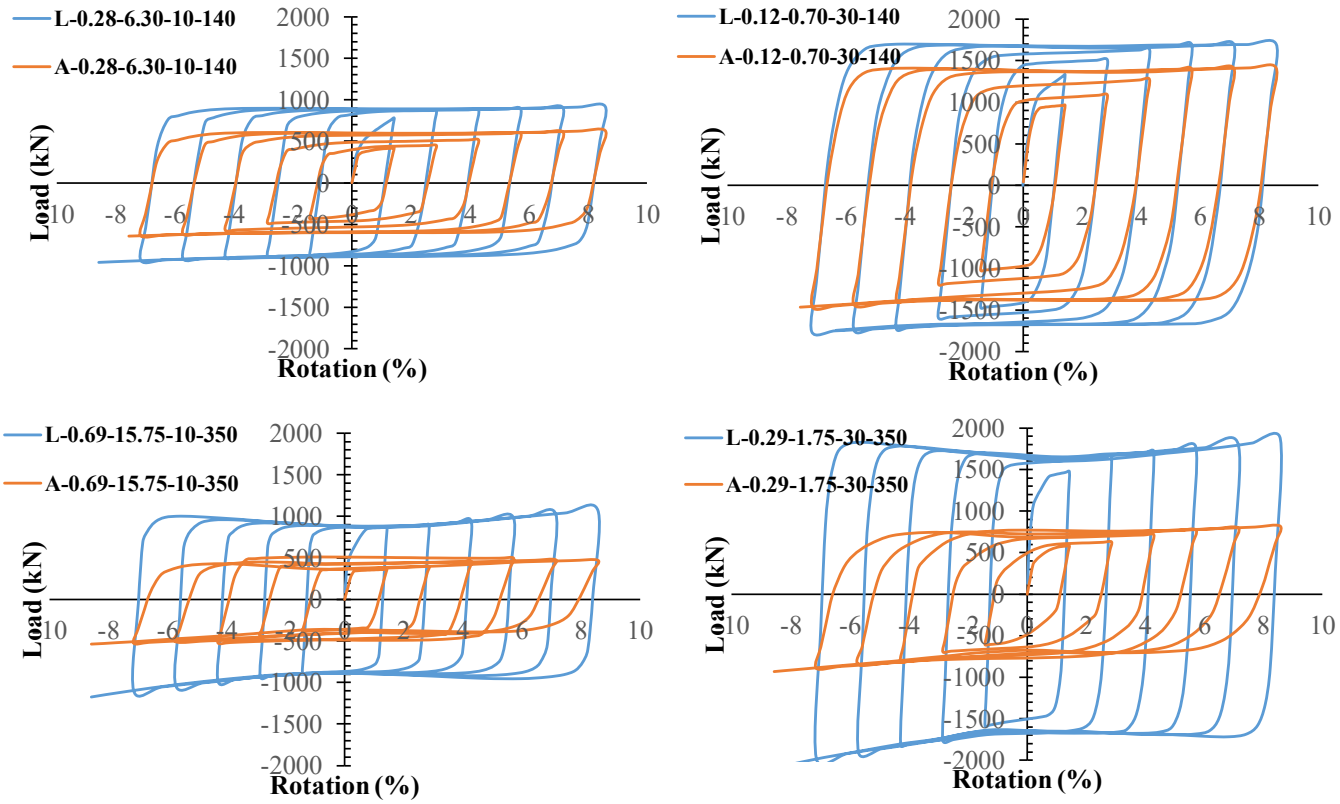

Figure 4. Comparing the hysteresis curve of the LYP and A36 dampers.

Comparing the hysteresis curves of the dampers shown in Figure 5 confirms that ρ and ψ affected the hysteresis curves. By reducing h and increasing the t_f, the hysteresis loop shows a better performance. As shown in this figure, by reducing ρ, the ultimate strength and stiffness of both LYP and A36 dampers are increased but the rate is different. The parameters are considered exactly in the next sections.

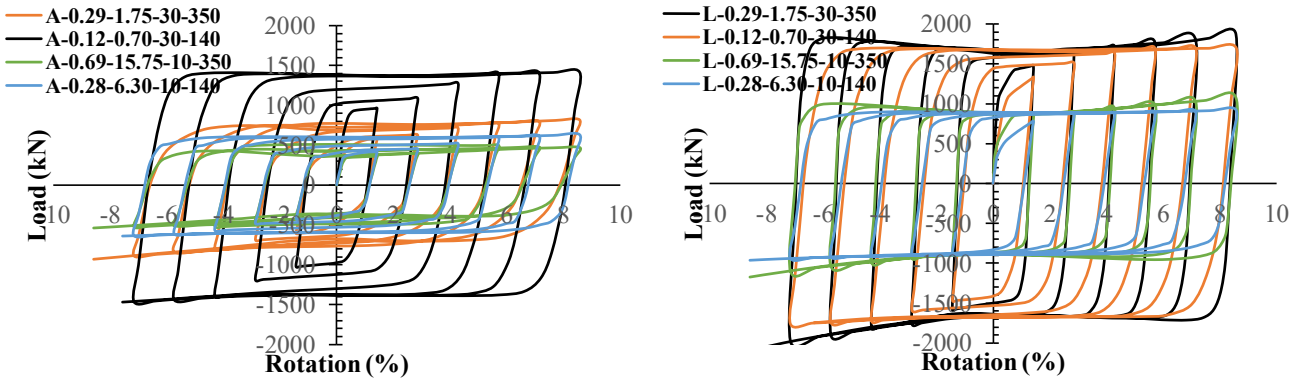

Figure 5. Comparing the hysteresis curve of the dampers.

6.2. Load-Rotation Curves

As described before, according to AISC 341-16, for a shear I-shaped link where $\rho < 1.6$, the nominal strength of the link is obtained as $V_n = 0.6F_{yw}A_w$, where in this I-shaped link $A_w = t_p b$. To have a better comparison of the performance of the damper, their load-rotation is plotted in Figure 6. Since in the analyzed dampers with LYP and A36 steel the $0.6F_{yw}A_w$ are the same, the same results are obtained according to the AISC 341-16. However, results displaced in Figure 6 reveal that, besides $0.6F_{yw}A_w$ and ρ, some other parameters affected the response of the I-shaped dampers. As shown in this figure, the V_n determined based on the AISC 341-16, although measured by the minimum shear strength of the I-shaped damper, it should be revised to predict the ultimate strength of the I-shaped damper. This figure also shows that in the same situation of $0.6F_{yw}A_w$, ρ, and ψ, the LYP dampers have a greater dissipating energy and ultimate strength.

6.3. Comparing the LYP and A36 Dampers

In Figure 7, the load-rotation of FE models with h = 140 mm and h = 350 mm are compared. In summary, other dampers are not shown, but all results are listed in Table 3. Results show that utilizing the LYP steel for the web plate made the curves rise, which caused an increase in the ultimate strength, dissipating energy, and stiffness. Moreover, in the A36 damper with a thinner flange plate, the Vn is close to $0.6F_{yw}A_w$, mainly in dampers with lower h; however, increasing the t_f causes an increase in the difference between the $0.6F_{yw}A_w$ and the ultimate strength of the dampers. This confirmed that the flange plate contributes to carrying the imposed load to the damper. Additionally, the equation predicts the minimum shear strength of the damper for a damper with higher h (and higher ρ). For the damper with lower h, the equation predicts the elastic zone with high error as minimum values of shear strength. Correspondingly, for all LYP dampers, the AISC recommendation predicts minimum values of the shear strength that is lower than the ultimate strength of the dampers.

Referring to Table 4, the LYP steel causes an improvement in the ultimate strength by 35% to 86%, elastic stiffness by 31% to 55%, overstrength by 40% to 68%, and the energy dissipation by 38% to 93%. Accordingly, the minimum improvement is attained by elastic stiffness and maximum enhancement is achieved by energy dissipation. The main feature of the paper is to increase the stiffness and dissipating energy of the damper by changing the materials of the web plate from A36 to LYP; the goal is obtained but the overstrength and ultimate strength are increased as well. The advantage of increasing the ultimate strength of the damper is reducing the required dampers in the structures, but increasing the overstrength has advantages and disadvantages.

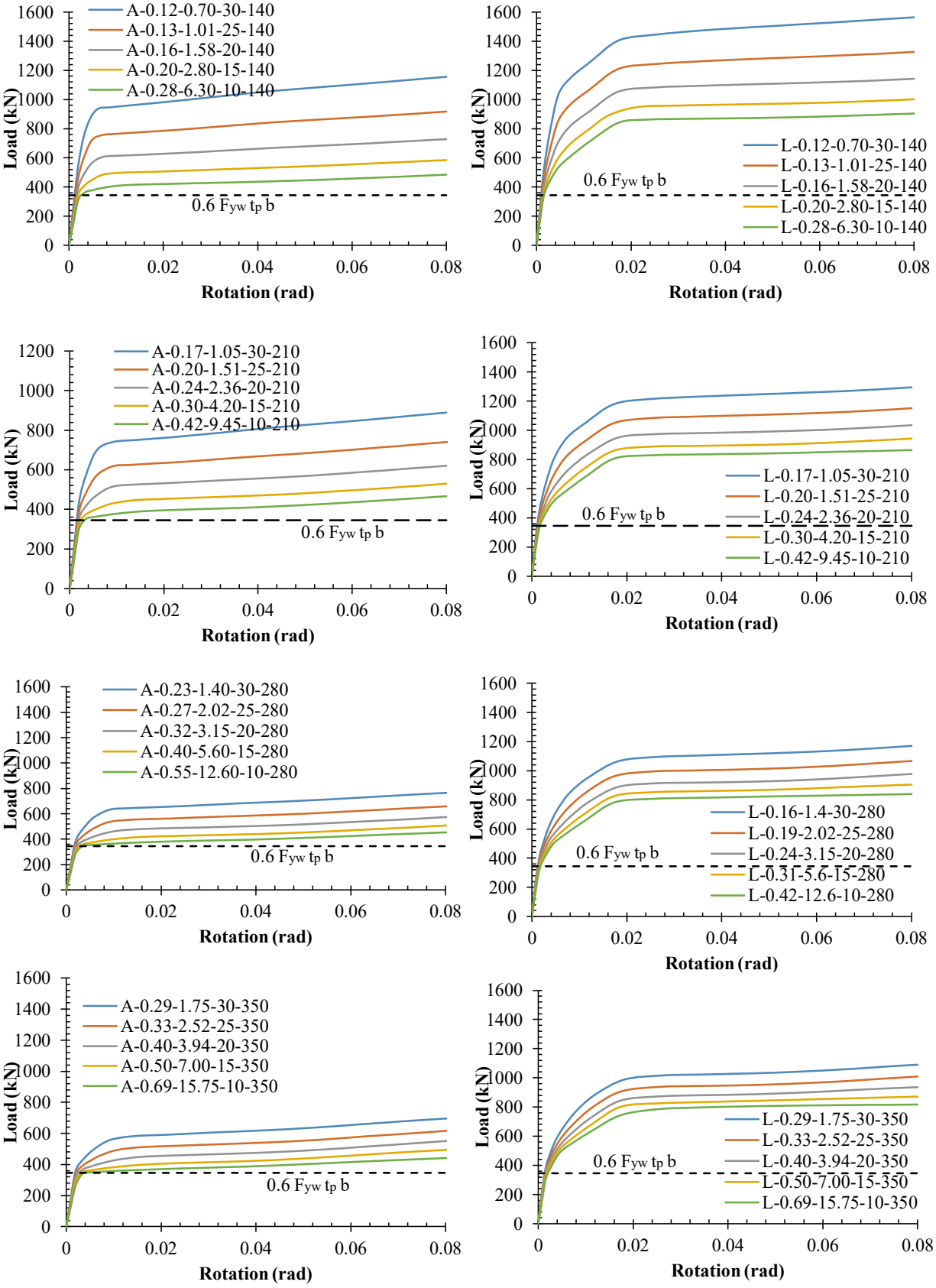

Figure 6. Load-rotation curves for FE models.

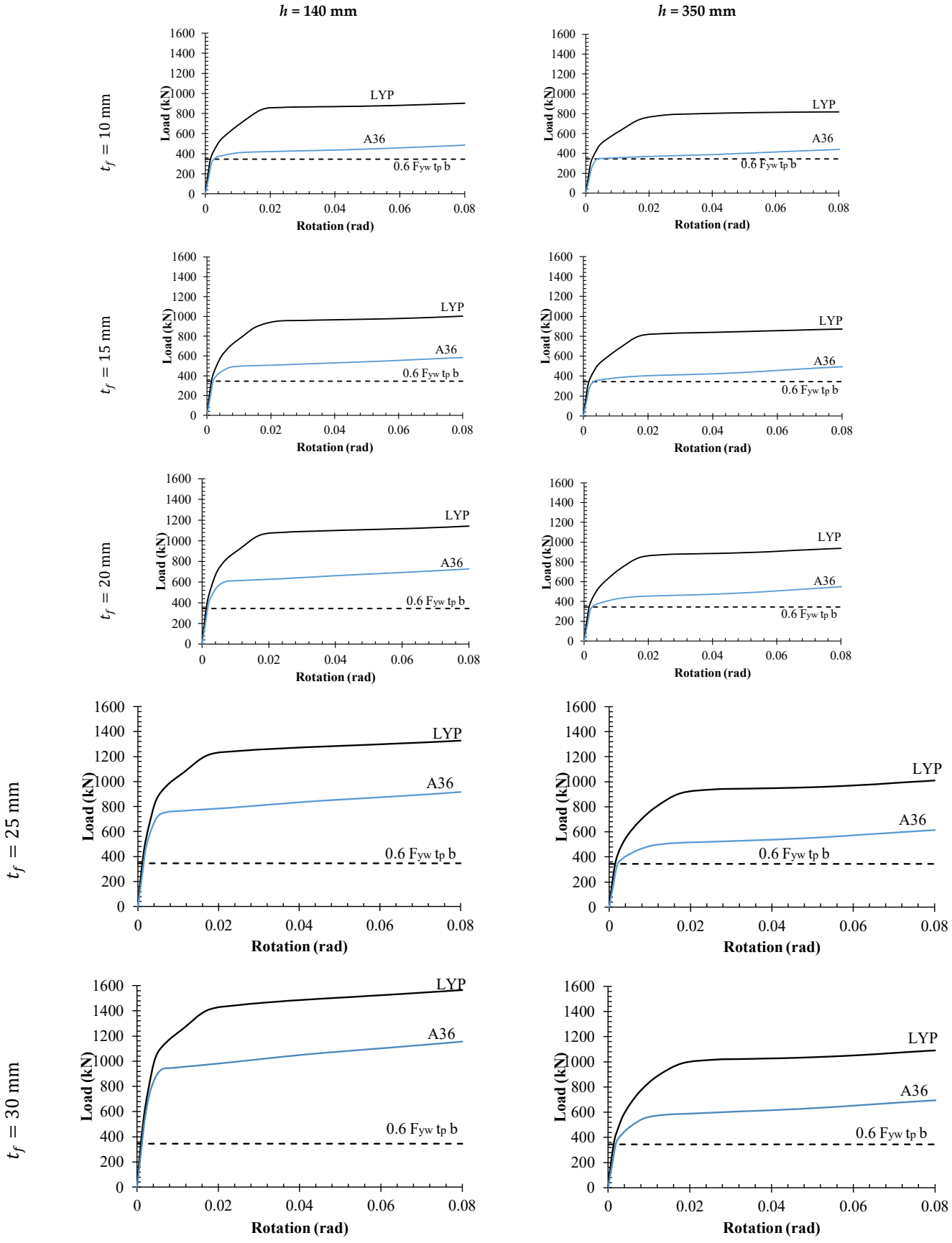

Figure 7. Comparing the load-rotation of damper with LYP and A36 steel for h = 140 mm and h = 350 mm.

Table 3. The structural parameters.

Model	ρ	ψ *	Ultimate Strength	Stiffness (kN/mm)	Δy ** (mm)	Over Strength	Energy Absorption (kN/mm)
L-0.28-6.30-10-140	0.28	6.30	903.00	1735.68	0.52	2.59	9154.45
L-0.20-2.80-15-140	0.20	2.80	1002.57	1885.95	0.53	2.67	10170.36
L-0.16-1.58-20-140	0.16	1.58	1141.08	2075.28	0.55	2.75	11592.49
L-0.13-1.01-25-140	0.13	1.01	1327.43	2315.11	0.57	2.83	13450.03
L-0.12-0.70-30-140	0.12	0.70	1565.01	2603.60	0.60	2.91	15757.71
L-0.42-9.45-10-210	0.42	9.45	864.87	1119.50	0.77	2.55	13199.68
L-0.30-4.20-15-210	0.30	4.20	943.12	1216.37	0.78	2.62	14192.51
L-0.24-2.36-20-210	0.24	2.36	1035.67	1315.03	0.79	2.71	15603.40
L-0.20-1.51-25-210	0.20	1.51	1151.15	1425.64	0.81	2.79	17415.94
L-0.17-1.05-30-210	0.17	1.05	1294.67	1554.17	0.83	2.86	19630.52
L-0.55-12.60-10-280	0.55	12.60	840.17	780.42	1.08	2.58	17146.26
L-0.40-5.60-15-280	0.40	5.60	903.26	858.92	1.05	2.61	18164.80
L-0.32-3.15-20-280	0.32	3.15	978.73	929.33	1.05	2.69	19510.22
L-0.27-2.02-25-280	0.27	2.02	1066.74	1000.04	1.07	2.77	21288.09
L-0.23-1.40-30-280	0.23	1.40	1171.13	1075.75	1.09	2.85	23483.36
L-0.69-15.75-10-350	0.69	15.75	817.28	567.65	1.44	2.65	20879.16
L-0.50-7.00-15-350	0.50	7.00	871.22	635.23	1.37	2.62	22043.02
L-0.40-3.94-20-350	0.40	3.94	936.96	692.19	1.35	2.68	23390.80
L-0.33-2.52-25-350	0.33	2.52	1008.55	745.70	1.35	2.75	25070.53
L-0.29-1.75-30-350	0.29	1.75	1090.51	799.23	1.36	2.83	27192.85
A-0.28-6.30-10-140	0.28	6.30	484.76	1126.24	0.43	1.54	4818.12
A-0.20-2.80-15-140	0.20	2.80	583.88	1254.71	0.47	1.67	5814.61
A-0.16-1.58-20-140	0.16	1.58	727.55	1437.60	0.51	1.82	7239.76
A-0.13-1.01-25-140	0.13	1.01	917.02	1684.32	0.54	1.95	9103.13
A-0.12-0.70-30-140	0.12	0.70	1155.30	1989.45	0.58	2.08	11409.81
A-0.42-9.45-10-210	0.42	9.45	465.46	722.55	0.64	1.53	6830.08
A-0.30-4.20-15-210	0.30	4.20	530.31	789.86	0.67	1.61	7790.79
A-0.24-2.36-20-210	0.24	2.36	620.16	868.41	0.71	1.75	9163.62
A-0.20-1.51-25-210	0.20	1.51	749.37	966.74	0.78	1.91	11761.62
A-0.17-1.05-30-210	0.17	1.05	888.29	1089.47	0.82	2.01	13171.23
A-0.55-12.60-10-280	0.55	12.60	455.72	511.26	0.89	1.59	9239.47
A-0.40-5.60-15-280	0.40	5.60	511.02	560.45	0.91	1.63	9922.06
A-0.32-3.15-20-280	0.32	3.15	581.32	609.31	0.95	1.74	11659.08
A-0.27-2.02-25-280	0.27	2.02	661.21	663.91	1.00	1.85	13189.83
A-0.23-1.40-30-280	0.23	1.40	773.43	727.96	1.06	2.00	16122.70
A-0.69-15.75-10-350	0.69	15.75	444.70	380.43	1.17	1.67	11286.43
A-0.50-7.00-15-350	0.50	7.00	498.51	421.27	1.18	1.69	12361.18
A-0.40-3.94-20-350	0.40	3.94	573.63	457.88	1.25	1.80	15725.37
A-0.33-2.52-25-350	0.33	2.52	621.87	495.27	1.26	1.84	15518.53
A-0.29-1.75-30-350	0.29	1.75	698.29	536.03	1.30	1.95	17326.80

* the ratio of the web plate capacity divided by the flange plate capacity. ** displacement corresponding to the yielding.

6.4. Influence of ρ on the Stiffness and Strength

As mentioned before, according to the AISC, I-shaped shear links with $\rho < 1.6$ act as shear mechanisms. However, many researchers [20,21,30] have been investigating links with $\rho < 1$ (very short links). They concluded that links with the same value of ρ (where $\rho < 1$) have the same elastic behavior and different nonlinear behavior. To do so, the ultimate strength and stiffness of dampers are plotted versus ρ in Figure 8. As shown in this figure, by increasing the ρ, the ultimate strength and stiffness of both LYP and A36 dampers are reduced but the rate is different. For the parameters after $\rho > 0.6$, the slope of reduction tends to be smooth. So, the following equations are proposed for the primary design of the damper:

$$K = 389\rho^{-0.85} \quad (10)$$

$$K = 241\rho^{-0.85} \tag{11}$$

and for ultimate strength

$$V_n = 679\rho^{-0.33} \tag{12}$$

$$V_n = 337.95\rho^{-0.48} \tag{13}$$

Table 4. The structural parameters of LYP damper divided by A36 damper.

	ρ	ψ *	tf ** (mm)	LYP Damper Divided by A36 Damper			
				Ultimate Strength	Stiffness	Over Strength	Energy Absorption
	0.28	6.30	10	1.86	1.54	1.68	1.90
	0.20	2.80	15	1.72	1.50	1.60	1.75
$h = 140$ mm	0.16	1.58	20	1.57	1.44	1.51	1.60
	0.13	1.01	25	1.45	1.37	1.45	1.48
	0.12	0.70	30	1.35	1.31	1.40	1.38
	0.42	9.45	10	1.86	1.55	1.66	1.93
	0.30	4.20	15	1.78	1.54	1.63	1.82
$h = 210$ mm	0.24	2.36	20	1.67	1.51	1.55	1.70
	0.20	1.51	25	1.54	1.47	1.46	1.48
	0.17	1.05	30	1.46	1.43	1.42	1.49
	0.55	12.60	10	1.84	1.53	1.62	1.86
	0.40	5.60	15	1.77	1.53	1.60	1.83
$h = 280$ mm	0.32	3.15	20	1.68	1.53	1.55	1.67
	0.27	2.02	25	1.61	1.51	1.50	1.61
	0.23	1.40	30	1.51	1.48	1.43	1.46
	0.69	15.75	10	1.84	1.49	1.59	1.85
	0.50	7.00	15	1.75	1.51	1.55	1.78
$h = 350$ mm	0.40	3.94	20	1.63	1.51	1.49	1.49
	0.33	2.52	25	1.62	1.51	1.50	1.62
	0.29	1.75	30	1.56	1.49	1.45	1.57

* the ratio of the web plate capacity divided by the flange plate capacity. ** the flange plate thickness.

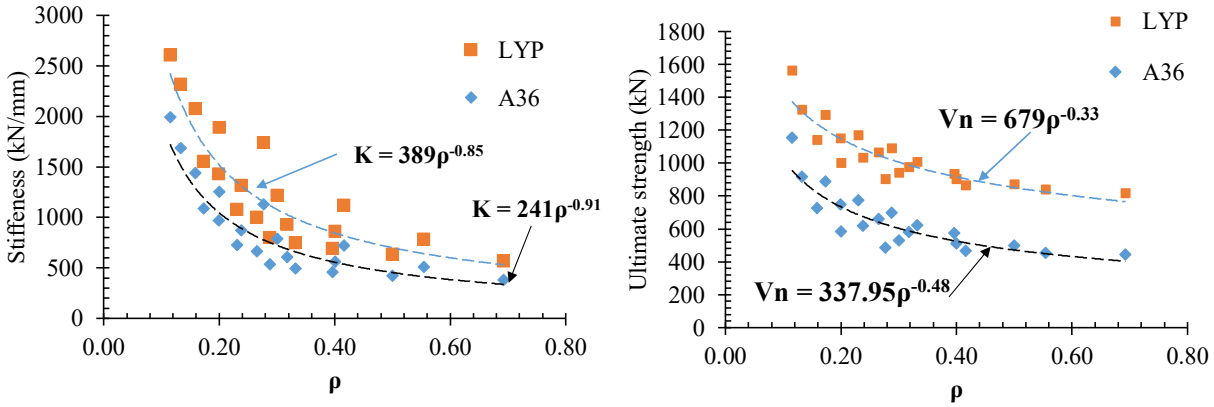

Figure 8. The ultimate strength and stiffness of dampers are plotted versus ρ.

Thus, this figure confirms that the load-rotation curve of the I-shaped damper is affected not only by the value of ρ but also by the value of ψ. As ψ decreases, the ultimate capacity of the damper increases. Thus, the contribution of the flange cannot be ignored when calculating the ultimate strength of the I-shaped damper.

6.5. Contribution of the Flange to Shear Strength

This section evaluates the relative contributions of the flange and the web to the performance of the damper. To do so, the load rotation of dampers for both LYP and A36 dampers with different h is plotted in Figure 9. Results indicate that in the elastic zone, web

plates of all dampers are the same contribution. Nevertheless, in the nonlinear zone, for both LYP and A36 damper, the flange plate contributes to the load carrying that is increased by increasing the t_f.

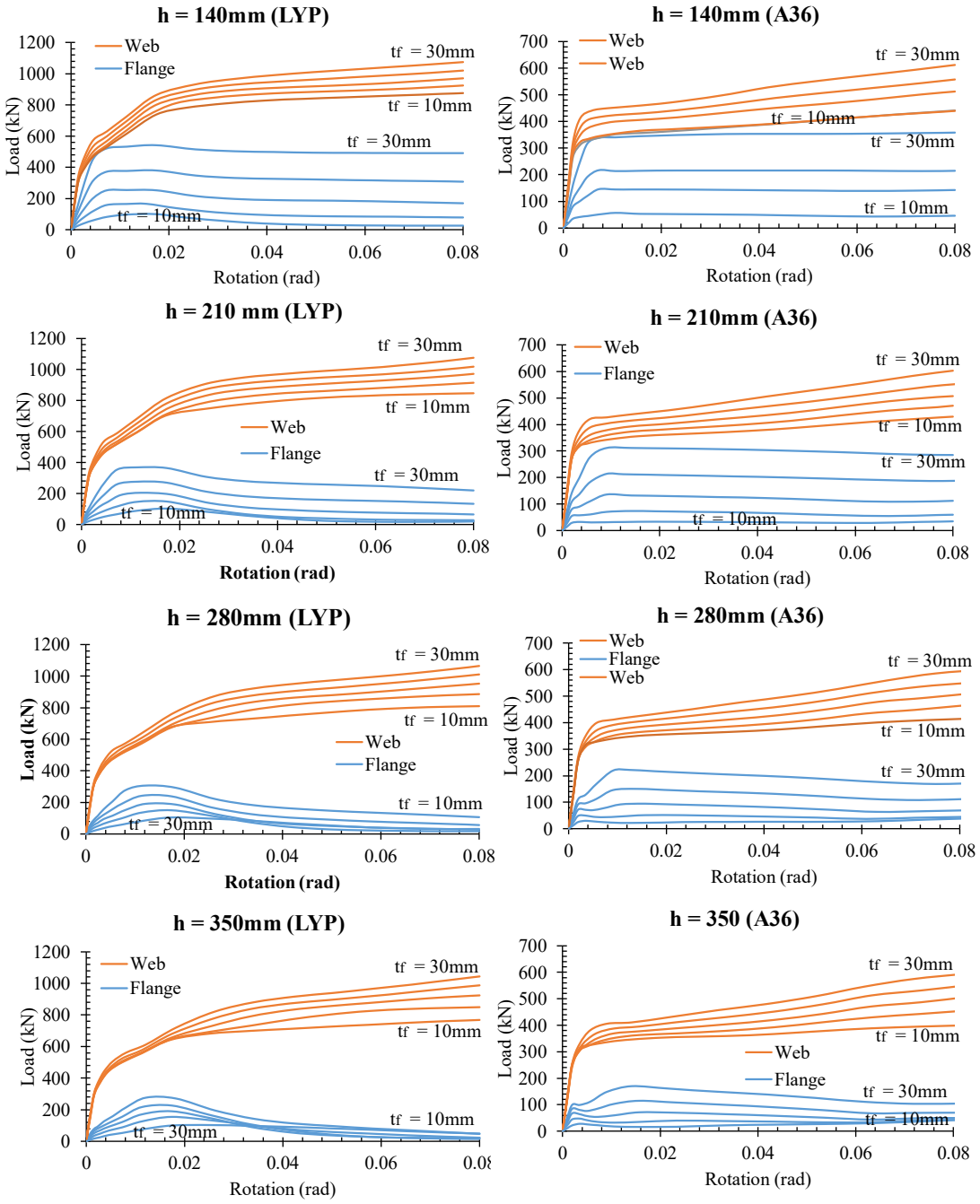

Figure 9. Contribution of the flange to the damper shear strength.

Although the same properties such as flange plates, web plate shear strength, and the ratio of web plate strength to flange plate strength are used for both LYP and A36 dampers, the contribution of the flange plate in the imposed load of A36 is greater than LYP dampers, due to the properties of LYP steel in the nonlinear zone.

Figure 10 and Table 5 show that, when b/h < 1 (h = 140 mm), the flange absorbs 7.62% to 31.29% (by increasing the t_f from 10 mm to 30 mm) at the beginning of loading and 2.93% to 31.67% at the end of loading for LYP dampers. For A36 dampers, the flange absorbs

11.07% to 41.60% (by increasing the t_f from 10 mm to 30 mm) at the beginning of loading and 9.38% to 47.07% at the end of loading.

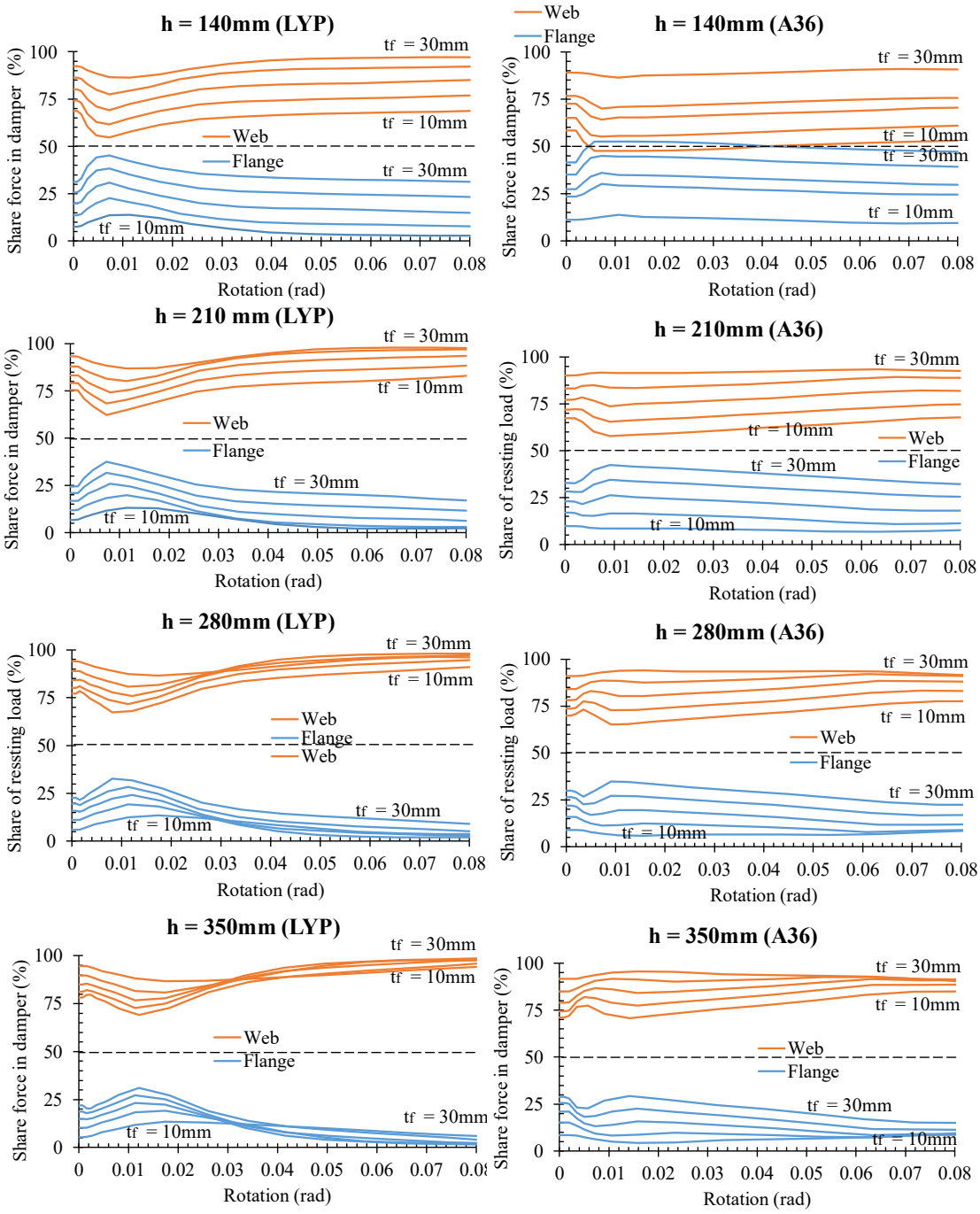

Figure 10. Share of load absorbed by the shear link flange and web for FE models (h-t_f-ρ-ψ).

Accordingly, by increasing the h to 350 mm (b/h > 1), the flange absorbs 5.42% to 21.86% (by increasing the t_f from 10 mm to 30 mm) at the beginning of loading and 6.64% to 6.45% at the end of loading for LYP dampers. For A36 dampers, the flange absorbs 15.1% to 28.9% (by increasing the t_f from 10 mm to 30 mm) at the beginning of loading and 8.86% to 15.01% at the end of loading.

Table 5. Comparing the contribution of the flange to the damper shear strength.

Model	ρ	ψ *	t_f ** (mm)	Rotation = 0		Rotation 8%	
				Flange Plate	Web Plate	Flange Plate	Web Plate
L-0.28-6.30-10-140	0.28	6.30	10	7.62	92.38	2.93	97.07
L-0.20-2.80-15-140	0.20	2.80	15	13.72	86.28	8.29	91.71
L-0.16-1.58-20-140	0.16	1.58	20	19.83	80.17	15.43	84.57
L-0.13-1.01-25-140	0.13	1.01	25	25.76	74.24	23.66	76.34
L-0.12-0.70-30-140	0.12	0.70	30	31.29	68.71	31.67	68.33
L-0.42-9.45-10-210	0.42	9.45	10	6.62	93.38	2.10	97.90
L-0.30-4.20-15-210	0.30	4.20	15	11.95	88.05	3.09	96.91
L-0.24-2.36-20-210	0.24	2.36	20	16.80	83.20	7.32	92.68
L-0.20-1.51-25-210	0.20	1.51	25	20.93	79.07	12.35	87.65
L-0.17-1.05-30-210	0.17	1.05	30	24.43	75.57	17.99	82.01
L-0.55-12.60-10-280	0.55	12.60	10	5.98	94.02	3.69	96.31
L-0.40-5.60-15-280	0.40	5.60	15	11.09	88.91	1.92	98.08
L-0.32-3.15-20-280	0.32	3.15	20	15.83	84.17	3.65	96.35
L-0.27-2.02-25-280	0.27	2.02	25	19.72	80.28	6.03	93.97
L-0.23-1.40-30-280	0.23	1.40	30	22.71	77.29	10.95	89.05
L-0.69-15.75-10-350	0.69	15.75	10	5.42	94.58	6.64	93.36
L-0.50-7.00-15-350	0.50	7.00	15	10.31	89.69	2.46	97.54
L-0.40-3.94-20-350	0.40	3.94	20	14.97	85.03	1.74	98.26
L-0.33-2.52-25-350	0.33	2.52	25	18.86	81.14	2.94	97.06
L-0.29-1.75-30-350	0.29	1.75	30	21.86	78.14	6.45	93.55
A-0.28-6.30-10-140	0.28	6.30	10	11.07	88.93	9.38	90.62
A-0.20-2.80-15-140	0.20	2.80	15	23.39	76.61	24.48	75.52
A-0.16-1.58-20-140	0.16	1.58	20	27.34	72.66	29.56	70.44
A-0.13-1.01-25-140	0.13	1.01	25	34.95	65.05	39.11	60.89
A-0.12-0.70-30-140	0.12	0.70	30	41.60	58.40	47.04	52.96
A-0.42-9.45-10-210	0.42	9.45	10	9.79	90.21	7.58	92.42
A-0.30-4.20-15-210	0.30	4.20	15	16.87	83.13	11.25	88.75
A-0.24-2.36-20-210	0.24	2.36	20	23.00	77.00	18.11	81.89
A-0.20-1.51-25-210	0.20	1.51	25	28.19	71.81	25.32	74.68
A-0.17-1.05-30-210	0.17	1.05	30	32.71	67.29	32.16	67.84
A-0.55-12.60-10-280	0.55	12.60	10	9.02	90.98	8.77	91.23
A-0.40-5.60-15-280	0.40	5.60	15	15.94	84.06	8.88	91.12
A-0.32-3.15-20-280	0.32	3.15	20	21.85	78.15	11.99	88.01
A-0.27-2.02-25-280	0.27	2.02	25	26.43	73.57	16.94	83.06
A-0.23-1.40-30-280	0.23	1.40	30	29.94	70.06	22.35	77.65
A-0.69-15.75-10-350	0.69	15.75	10	8.35	91.65	9.98	90.02
A-0.50-7.00-15-350	0.50	7.00	15	15.10	84.90	8.61	91.39
A-0.40-3.94-20-350	0.40	3.94	20	21.00	79.00	8.81	91.19
A-0.33-2.52-25-350	0.33	2.52	25	25.58	74.42	11.23	88.77
A-0.29-1.75-30-350	0.29	1.75	30	28.90	71.10	15.01	84.99

* the ratio of the web plate capacity divided by the flange plate capacity. ** the flange plate thickness.

It is concluded, that for LYP dampers, the flange plate contribution in the shear strength of the damper is ignorable at the beginning of imposed loading. Additionally, for thin flange plates, the effect of the flange plate on the shear strength can be ignored, which may give low errors of less than 8%. However, the effect of the flange plate on the response of the A36 damper is considerable.

6.6. Effect of the Flange on the Damper Response

To consider the effect of the flange plate on the response of the dampers with different t_f, (t_f = i) divided by t_f = 10 mm are listed in Table 6. Results reveal that while the t_f is increased, the Vn, K, Ω, and E are improved; this improvement is related to the h reduction as well. Referring to the results, both dampers' parameters are increased by growing the t_f and reducing h. This confirms that the increasing parameters of the damper are related to the stiffness of the flange plate (that contains t_f and h). For LYP dampers, the maximum

improvement of the parameters Vn, K, Ω, and E for h = 140 mm and h = 350 mm are, respectively, 73% and 33%, 50% and 41%, 12% and 6%, and 72% and 30%. For A36, this is 2.38 times and 57%, 77% and 41%, 35% and 16%, and 2.38 times and 54%. Moreover, the A36 damper is more affected by the flange plate stiffness than the LYP damper.

Table 6. Comparing the parameters damper with different t_f with t_f = 10 mm.

Model	ρ	ψ *	tf ** (mm)	damper with $\frac{t_f=i}{t_f=10mm}$			
				Ultimate Strength	Stiffness	Over Strength	Energy Absorption
L-0.28-6.30-10-140	0.28	6.30	10				
L-0.20-2.80-15-140	0.20	2.80	15	1.11	1.09	1.03	1.11
L-0.16-1.58-20-140	0.16	1.58	20	1.26	1.20	1.06	1.27
L-0.13-1.01-25-140	0.13	1.01	25	1.47	1.33	1.09	1.47
L-0.12-0.70-30-140	0.12	0.70	30	1.73	1.50	1.12	1.72
L-0.42-9.45-10-210	0.42	9.45	10				
L-0.30-4.20-15-210	0.30	4.20	15	1.09	1.09	1.03	1.08
L-0.24-2.36-20-210	0.24	2.36	20	1.20	1.17	1.06	1.18
L-0.20-1.51-25-210	0.20	1.51	25	1.33	1.27	1.09	1.32
L-0.17-1.05-30-210	0.17	1.05	30	1.50	1.39	1.12	1.49
L-0.55-12.60-10-280	0.55	12.60	10				
L-0.40-5.60-15-280	0.40	5.60	15	1.08	1.10	1.01	1.06
L-0.32-3.15-20-280	0.32	3.15	20	1.16	1.19	1.04	1.14
L-0.27-2.02-25-280	0.27	2.02	25	1.27	1.28	1.07	1.24
L-0.23-1.40-30-280	0.23	1.40	30	1.39	1.38	1.10	1.37
L-0.69-15.75-10-350	0.69	15.75	10				
L-0.50-7.00-15-350	0.50	7.00	15	1.07	1.12	0.99	1.06
L-0.40-3.94-20-350	0.40	3.94	20	1.15	1.22	1.01	1.12
L-0.33-2.52-25-350	0.33	2.52	25	1.23	1.31	1.04	1.20
L-0.29-1.75-30-350	0.29	1.75	30	1.33	1.41	1.06	1.30
A-0.28-6.30-10-140	0.28	6.30	10				
A-0.20-2.80-15-140	0.20	2.80	15	1.20	1.11	1.08	1.21
A-0.16-1.58-20-140	0.16	1.58	20	1.50	1.28	1.18	1.50
A-0.13-1.01-25-140	0.13	1.01	25	1.89	1.50	1.27	1.89
A-0.12-0.70-30-140	0.12	0.70	30	2.38	1.77	1.35	2.37
A-0.42-9.45-10-210	0.42	9.45	10				
A-0.30-4.20-15-210	0.30	4.20	15	1.14	1.09	1.05	1.14
A-0.24-2.36-20-210	0.24	2.36	20	1.33	1.20	1.14	1.34
A-0.20-1.51-25-210	0.20	1.51	25	1.61	1.34	1.25	1.72
A-0.17-1.05-30-210	0.17	1.05	30	1.91	1.51	1.31	1.93
A-0.55-12.60-10-280	0.55	12.60	10				
A-0.40-5.60-15-280	0.40	5.60	15	1.12	1.10	1.02	1.07
A-0.32-3.15-20-280	0.32	3.15	20	1.28	1.19	1.09	1.26
A-0.27-2.02-25-280	0.27	2.02	25	1.45	1.30	1.16	1.43
A-0.23-1.40-30-280	0.23	1.40	30	1.70	1.42	1.25	1.74
A-0.69-15.75-10-350	0.69	15.75	10				
A-0.50-7.00-15-350	0.50	7.00	15	1.12	1.11	1.01	1.10
A-0.40-3.94-20-350	0.40	3.94	20	1.29	1.20	1.07	1.39
A-0.33-2.52-25-350	0.33	2.52	25	1.40	1.30	1.10	1.37
A-0.29-1.75-30-350	0.29	1.75	30	1.57	1.41	1.16	1.54

* the ratio of the web plate capacity divided by the flange plate capacity. ** the flange plate thickness.

In Figure 11, the maximum increasing of the parameters Vn, Ω, and E due to increasing the t_f are plotted versus the h. This figure shows that A36 has more sensitive flange plate properties than LYP. Additionally, the Vn and E have a greater increase, whereas the Ω has a lower sensitivity to the flange plate properties.

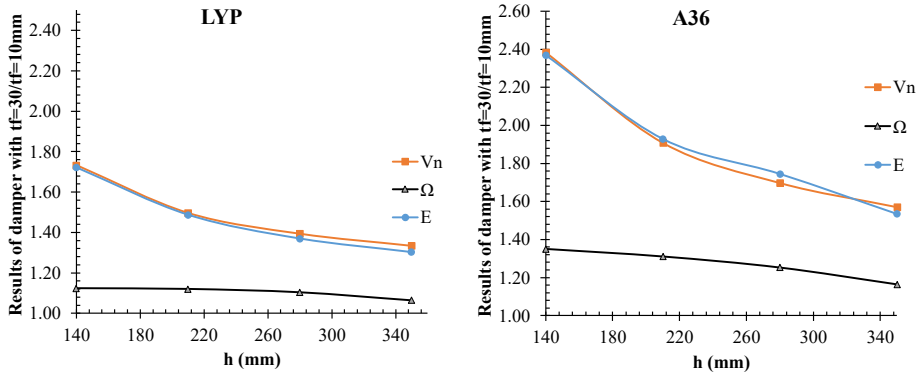

Figure 11. The maximum increase of Vn, Ω, and E versus h.

To have a better comparison, the Ω and Vn versus ψ are plotted in Figure 12. Since other parameters K and E did not show a specific relation with ψ, they are not plotted. As shown in this figure, during $\psi < 1$, the Vn is suddenly dropped and during $1 < \psi < 2$, the rate of reduction is reduced. Additionally, by $\psi > 2$, the effect of the flange plate on the Vn is ignorable. Therefore, it is recommended to design the damper with $\psi > 2$ to reduce the sensitivity of the Vn to the flange plate properties. However, for Ω, the lower sensitivity value is obtained related to the ψ, but the minim value is occurring around $\psi = 10$. Since the element outside the damper must be designed for ΩVn, lower Ω helps to reduce the construction cost.

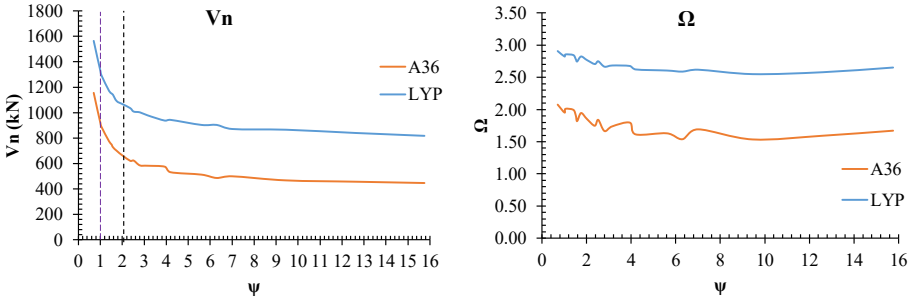

Figure 12. The Ω and Vn versus ψ for LYP and A36 dampers.

7. Conclusions

In this paper, an innovative I-shaped damper with a shear mechanism made of LYP steel for web plates and A36 for flange plates was investigated numerically and parametrically. The main feature of using LYP steel for web plate was to increase energy absorption and stiffness. The finding is summarized as follows:

- Both dampers with LYP steel and A36 steel pertain to stable hysteresis loops without any degradation, which confirms the capability of the I-shaped damper to dissipate seismic energy.
- Besides the web plate shear strength as $0.6F_{yw}A_w$ and ρ parameter, some other parameters affect the response of the I-shaped dampers. The V_n was determined based on the AISC 341-16 and, although it measured the minimum shear strength of the I-shaped damper, it should be revised to predict the ultimate strength of the I-shaped damper. In the same situation of $0.6F_{yw}A_w$, ρ, and ψ, the LYP dampers have a greater dissipating energy and ultimate strength.
- Results reveal that while t_f is increased, the Vn, K, Ω, and E are improved, however this improvement is related to the h reduction as well. Moreover, the A36 damper is more affected by the flange plate stiffness than the LYP damper.
- It is concluded that, for the LYP damper, the flange plate contribution in the shear strength of the damper is ignorable at the beginning of imposed loading. Additionally, for a thin flange plate, the effect of the flange plate on the shear strength can be ignored,

which may give low errors of less than 8%. However, the effect of the flange plate on the response of the A36 damper is not ignorable.

- Increasing the parameters of the damper is related to the stiffness of the flange plate. For the LYP damper, the maximum improvement of the parameters Vn, K, Ω, and E for h = 140 mm and h = 350 mm are, respectively, 73% and 33%, 50% and 41%, 12% and 6%, and 72% and 30%. For A36, this is 2.38 times and 57%, 77% and 41%, 35% and 16%, and 2.38 times and 54%.
- Since by $\psi < 1$, the Vn is dropped and through the $1 < \psi < 2$ and $\psi > 2$, respectively, the rate of reduction is reduced and the effect of the flange plate on the Vn is ignorable, the design of a damper with $\psi > 2$ is suggested to reduce the sensitivity of the Vn to the flange plate properties.
- The minim value of Ω is obtained around $\psi = 10$. Since the element outside the damper must be designed for ΩVn, a lower Ω helps to reduce the construction cost.
- Recommendations for future work: It is suggested that a comprehensive study be conducted regarding the damper when it is made of A36 steel or LYP steel (for web or all components of the damper) from the economic aspect and to examine the construction costs. In this case, various parameters, including the number of stories, as well as the optimal mode of using this damper, can be obtained.

Author Contributions: Conceptualization, A.G., R.P.J. and C.T.; methodology, A.G., R.P.J. and T.S.; software, A.G.; validation, A.G. and C.T.; formal analysis, A.G.; investigation, A.G. and C.T.; resources, R.P.J.; data curation, C.T. and T.S.; writing—original draft preparation, A.G.; writing—review and editing, R.P.J.; visualization, A.G.; supervision, R.P.J.; project administration, A.G.; funding acquisition, R.P.J. All authors have read and agreed to the published version of the manuscript.

Funding: this research was funded by Universiti Malaysia Pahang: PDU213219.

Institutional Review Board Statement: Not applicable.

Informed Consent Statement: Not applicable.

Data Availability Statement: Not applicable.

Acknowledgments: This research was supported by the Thammasat University Research Unit in Structural and Foundation Engineering, Thammasat University. In addition, this work was supported by the Thailand Science Research and Innovation Fundamental Fund fiscal year 2023.

Conflicts of Interest: The authors declare no conflict of interest.

Abbreviations

b	web Length of I-shaped link	M_{pf}	plastic moment of the flange plate
d	depth of I-shaped link	R_{yw}	ratios of the expected yield stress to the specified minimum yield stress for the web
e	link length	R_{yf}	ratios of the expected yield stress to the specified minimum yield stress for the flange
E	modulus of elasticity	t_f	flange plate thickness
h	height of link	t_p	web plate thickness
K	the coefficient for the effective length	V_{design}	design force
L	length	V_s	loads corresponding to the start of the nonlinear zone
r	radius of gyration	V_f	shear strength of the flange plate
V	lateral shear applied to the structure	V_P	plastic shear capacity
A_w	web area section	V_u	ultimate strength
b_f	flange width	Φ	the compressive strength reduction coefficient
F_y	yield stress of the brace	Ω	over strength
F_{yw}	web yield stress	ρ	link length ratio
F_{yf}	yield stress of the flange plates	ϕ_v	shear resistance coefficient
V_n	nominal shear strength	α	the angle of the diagonal brace element relative to the horizontal
M_P	plastic moment capacity		

References

1. Yang, T.Y.; Neitsch, J.; Al-Janabi, M.A.Q.; Tung, D.P. Seismic performance of eccentrically braced frames designed by the conventional and equivalent energy procedures. *Soil Dyn. Earthq. Eng.* **2020**, *139*, 106322. [CrossRef]
2. Ghaedi, K.; Ibrahim, Z.; Javanmardi, A.; Rupakhety, R. Experimental study of a new bar damper device for vibration control of structures subjected to earthquake loads. *J. Earthq. Eng.* **2018**, *25*, 300–318. [CrossRef]
3. Engelhardt, M.D.; Popov, E.P. Experimental performance of long links in eccentrically braced frames. *J. Struct. Eng.* **1992**, *118*, 3067–3088. [CrossRef]
4. Nuzzo, I.; Losanno, D.; Serino, G.; Bozzo, L. A seismic resistant precast RC system equipped with shear link dissipators for residential buildings. In Proceedings of the Second International Conference on Advances in Civil, Structural and Environmental Engineering, Zurich, Switzerland, 25–26 October 2014; Volume 2, pp. 249–254. [CrossRef]
5. Mohsenian, V.; Hajirasouliha, I.; Filizadeh, R. Seismic reliability analysis of steel moment-resisting frames retrofitted by vertical link elements using combined series–parallel system approach. *Bull. Earthq. Eng.* **2021**, *19*, 831–862. [CrossRef]
6. Corte, D.; D'Aniello, M.; Landolfo, R. Analytical and numerical study of plastic overstrength of shear links. *J. Constr. Steel Res.* **2013**, *82*, 19–32. [CrossRef]
7. Ji, X.; Wang, Y.; Ma, Q.; Okazaki, T. Cyclic behavior of very short steel shear links. *J. Struct. Eng.* **2016**, *142*, 04015114. [CrossRef]
8. Bozkurt, M.; Topkaya, C. Replaceable links with gusseted brace joints for eccentrically braced frames. *Soil Dyn. Earthq. Eng.* **2018**, *115*, 305–318. [CrossRef]
9. Chesoan, A.; Stratan, A.; Dubina, D. Design implementation of re-centring dual eccentrically braced frames with removable links. *Soil Dyn. Earthq. Eng.* **2018**, *112*, 174–184. [CrossRef]
10. Zahrai, S.M.; Parsa, A. Effect of flange width of vertical link beam on cyclic behavior of chevron braced steel frames. *J. Seismol. Earthq. Eng.* **2015**, *17*, 281–292.
11. Valente, M.; Milani, G. Alternative retrofitting strategies to prevent the failure of an underdesigned reinforced concrete frame. *Eng. Fail. Anal.* **2018**, *89*, 271–285. [CrossRef]
12. Mazzolani, F.M.; Corte, G.D.; D'Aniello, M. Experimental analysis of steel dissipative bracing systems for seismic upgrading. *J. Civ. Eng. Manag.* **2009**, *15*, 7–19. [CrossRef]
13. Najari Varzaneh, M.; Hosseini, M.; Akbarpoor, A. The Study of EADAS Elliptical Steel Damper Function in Seismic Resisting of Steel Frames. *J. Rehabil. Civ. Eng.* **2014**, *2*, 40–45.
14. Shih, M.-H.; Sung, W.-P.; Go, C.-G. Investigation of newly developed added damping and stiffness device with low yield strength steel. *J. Zhejiang Univ. Sci.* **2004**, *5*, 326–334. [CrossRef] [PubMed]
15. Shojaeifara, H.; Maleki, A.; Lotfollahi-Yaghin, A. Performance Evaluation of Curved-TADAS Damper on Seismic Response of Moment Resisting Steel Frame. *Int. J. Eng.* **2020**, *33*, 55–67.
16. Özkaynak, H. Model Proposal for Steel Cushions for Use in Reinforced Concrete Frames. *KSCE J. Civ. Eng.* **2017**, *21*, 2717–2727. [CrossRef]
17. Miao, F.; Nejati, F.; Zubair, S.A.M.; Yassin, M.E. Seismic Performance of Eccentrical Braced Frame Retrofitted by Box Damper in Vertical Links. *Buildings* **2022**, *12*, 1506. [CrossRef]
18. Helm, L.; Sadegh-Azar, H.; Jahnel, L.; Jandrey, H. Application and Optimization of Ring Spring Dampers for Seismic Design. In Proceedings of the 10th International Conference on Behaviour of Steel Structures in Seismic Areas, Timisoara, Romania, 25–27 May 2022; STESSA 2022; Lecture Notes in Civil Engineering. Mazzolani, F.M., Dubina, D., Stratan, A., Eds.; Springer International Publishing: Cham, Switzerland, 2022. Note No. 262. [CrossRef]
19. Sahoo, D.R.; Singhal, T.; Taraithia, S.; Saini, A. Cyclic behavior of shear-and-flexural yielding metallic dampers. *J. Constr. Steel Res.* **2015**, *114*, 247–257. [CrossRef]
20. Ghamari, A.; Kim, C.-H.; Jeong, S.-H.; Hong, K.-J. Development of an innovative metallic damper for concentrically braced frame systems based on experimental and analytical studies. *Struct. Des. Tall Spec. Build.* **2022**, *31*, e1927. [CrossRef]
21. Ghamari, A.; Almasi, B.; Kim, C.-H.; Jeong, S.-H.; Hong, K.-J. An Innovative Steel Damper with a Flexural and Shear–Flexural Mechanism to Enhance the CBF System Behavior: An Experimental and Numerical Study. *Appl. Sci.* **2021**, *11*, 11454. [CrossRef]
22. Thongchom, C.; Bahrami, A.; Ghamari, A.; Benjeddou, O. Performance Improvement of Innovative Shear Damper Using Diagonal Stiffeners for Concentrically Braced Frame Systems. *Buildings* **2022**, *12*, 1794. [CrossRef]
23. Thongchom, C.; Ghamari, A.; Putra Jaya, R.; Benjeddoud, O. Experimental and Numerical Study on an Innovative Trapezoidal-Shaped Damper to Improve the Behavior of CBF Braces. *Buildings* **2023**, *13*, 140. [CrossRef]
24. Giannuzzi, D.; Ballarini, R.; Huckelbridge, A.; Pollino, M.; Valente, M. Braced Ductile Shear Panel: New Seismic-Resistant Framing System. *J. Struct. Eng.* **2014**, *140*, 04013050. [CrossRef]
25. Tanaka, T.; Sasaki, Y. Hysteresis Performance of Shear Panel Dampers of Ultra Low Yield Strength Steel for Seismic Response Control of Building. In Proceedings of the 12th World Conference on Earthquake Engineering, Auckland, New Zealand, 30 January–4 February 2000.
26. Choi, J.; Abebe, D. Hysteresis Characteristics of Shear Panel Damper Using SLY120. *APCBEE Procedia* **2014**, *9*, 370–375. [CrossRef]
27. Okazaki, T.; Engelhardt, M.D. Cyclic loading behavior of EBF links constructed of ASTM A992 steel. *J. Constr. Steel Res.* **2007**, *63*, 751–765. [CrossRef]
28. AISC. *AISC 341-16*; Seismic Provisions for Structural Steel Buildings. American Institute of Steel Construction: Chicago, IL, USA, 2016.

29. *ANSI/AISC 360-16*; Specification for Structural Steel Buildings. American Institute of Steel Construction: Chicago, IL, USA, 2016; pp. 1–612.
30. Ghadami, A.; Pourmoosavi, G.; Ghamari, A. Seismic design of elements outside of the short low-yield-point steel shear links. *J. Constr. Steel Res.* **2021**, *178*, 106489. [CrossRef]
31. Sabouri-Ghomi, S.; Ziaei, M. A study on the behavior of shear link beam made of easy-going steel in eccentrically braced frames. In Proceedings of the 14th World Conference on Earthquake Engineering, Beijing, China, 12–17 October 2008.
32. Dusicka, P.; Itani, A.M.; Buckle, I.G. Cyclic behavior of shear links of various grades of plate steel. *J. Struct. Eng.* **2010**, *136*, 370–378. [CrossRef]
33. Kasai, K.; Popov, E.P. *A Study of Seismically Resistant Eccentrically Braced 418 Frames*; Rep. No. UCB/EERC-86/01; Earthquake Engineering Research Center, University of California: Berkeley, CA, USA, 1983.
34. Hjelmstad, K.D.; Popov, E.P. *Seismic Behavior of Active Beam Link in Eccentrically Braced Frames*; Rep. No. UCB/EERC-83/15; Earthquake Engineering Research Center, University of California: Berkeley, CA, USA, 1983.
35. Engelhardt, M.D.; Popov, E.P. *Behavior of Long Links in Eccentrically Braced Frames*; Rep. No. UCB/EERC-89/01; Earthquake Engineering Research Center, University of California: Berkeley, CA, USA, 1989.
36. Okazaki, T.; Engelhardt, M.D.; Drolias, A.; Schell, E.; Hong, J.K.; Uang, C.M. Experimental investigation of link-to-column connections in eccentrically braced frames. *J. Constr. Steel Res.* **2009**, *65*, 1401–1412. [CrossRef]
37. McDaniel, C.C.; Uang, C.M.; Seible, F. Cyclic testing of built-up steel shear links for the new bay bridge. *J. Struct. Eng.* **2003**, *129*, 801–809. [CrossRef]
38. Manheim, D.N.; Popov, E.P. Plastic shear hinges in steel frames. *J. Struct. Eng.* **1983**, *10*, 2404–2419. [CrossRef]
39. Richards, P.W. Cyclic Stability and Capacity Design of Steel Eccentrically Braced Frames. Ph.D. Thesis, Department of Structural Engineering, University of California, San Diego, CA, USA, 2004.
40. Applied Technology Council (ATC). *Guildlines for Cyclic Seismic Testing of Component for Steel Structures*; ATC-24 Report; Applied Technology Council (ATC): Redwood City, CA, USA, 1992.